A robust multi-layer finite volume solver for density-driven shallow water flows

Fayssal Benkhaldoun [a], Saida Sari [a,*], Mohammed Seaïd [b],

[a] *LAGA, Université Paris* 13, 99 *Av J.B. Clement,* 93430 *Villetaneuse, France*

[b] *School of Engineering and Computing Sciences, University of Durham, South Road, DH1 3LE, UK*

Abstract

A robust solver is proposed for the numerical solution of density-driven multi-layer shallow water flows. The governing equations consist on coupling the multi-layer shallow water equations for the hydraulic variables with suspended sediment transport equations for the concentration variables. The layers can be formed in the shallow water model based on the variation of water density which may depend on the water temperature and salinity. At each time step, the method consists of two stages to update the numerical solution. In the first stage, the multi-layer shallow water equations are rewritten in a non-conservative form and the intermediate solutions are calculated using the modified method of characteristics. In the second stage, the numerical fluxes are reconstructed from the intermediate solutions in the first stage and used in the conservative form of the multi-layer shallow water equations. The proposed method avoids Riemann problem solvers and it is suitable for multi-layer shallow water equations on non-flat topography. Several numerical results are presented to illustrate the performance of the proposed finite volume method. The computed results confirm its capability to solve multi-layer shallow water equations for density-driven flows over flat and non-flat bottom topography.

Key words: Multi-layer shallow water equations, Density-driven flows, Finite volume method, Modified method of characteristics

1 Introduction

Mathematical modelling of water flows in the hydraulics and oceanic systems is based on the formulation and solution of the appropriate equations of continu-

* Corresponding author.
Email address: sari@math.univ-paris13.fr (Saida Sari).

ity and motion of water. In general, water flows represent a three-dimensional turbulent Newtonian flow in complicated geometrical domains. The cost of incorporating three-dimensional data in natural water courses is often excessively high. Computational efforts needed to simulate three-dimensional turbulent flows can also be significant. In view of such considerations, many researchers have tended to use rational approximations in order to develop two-dimensional hydrodynamical models for shallow water flows. Indeed, under the influence of gravity, many free-surface water flows can be modelled by the shallow water equations with the assumption that the vertical scale is much smaller than any typical horizontal scale. These equations can be derived from the depth-averaged incompressible Navier-Stokes equations using appropriate free-surface and boundary conditions along with a hydrostatic pressure assumption. The shallow water equations in depth-averaged form have been successfully applied to many engineering problems and their application fields include a wide spectrum of phenomena other than water waves. For instance, the shallow water equations have applications in environmental and hydraulics engineering such as tidal flows in an estuary or coastal regions, rivers, reservoir and open channel flows. Such practical flow problems are not trivial to simulate since the geometry can be complex and the topography irregular. However, single-layer shallow water equations have the drawback of missing some physical dynamics in the vertical motion. Therefore, during the last decades, multi-layer shallow water models have been attracted more attention and have became a very useful tools to solve hydrodynamical flows such as rivers, estuaries, bays and other nearshore regions where water flows interact with the bed geometry and wind shear stresses, see for instance [4,6,2]. The main advantage of these models is the fact that the multi-layer shallow water model avoids the expensive three-dimensional Navier-Stokes equations and obtains stratified horizontal flow velocities as vertical velocities are relatively small and the flow is still within the shallow water regime.

The multi-layer models studied in [4,6] among others, account only for the vertical variation of the density between the water layers. This makes their application very restrictive and can not be used to model density-driven flows where a horizontal variation in the water density is required for their dynamics. Recently, a single-layer model has been presented in [5] for shallow water flows with variable horizontal density. It has been shown in [5] that the governing equations form a hyperbolic system of conservation laws and can be used to model dam-break type problems where the water dynamics is controlled by the variation of water densities rather than the variation in water heights. The drawback of this model remains the failure to capture the vertical effects in the water dynamics. This water dynamics is refereed to by density-driven flow and it occurs in many applications such as ocean circulation, incursion of salty water in rivers at the sea-river intersections, and lock-exchange hydraulics for water bodies at different temperature. Our objective in this study is therefore, to develop a multi-layer model for shallow water flows with variable horizontal

or/and vertical density. It should be stressed that a multi-layer model for shallow water flows with variable density has been recently proposed in [1]. The model uses a single variable to represent the water height in the system. This fact limits the application of the model in [1] since the formation of the layers is artificial and has to exactly follow the bed profile. In our model we use different water density and water height at each layer, and it can be applied to arbitrary number and profile of the layers in the considered water system.

Numerical treatment of the multi-layer shallow water equations often presents difficulties due to their nonlinear form, presence of the source terms, coupling between the free-surface equation and the equations governing the water flow, compare [6,1] among others. In addition, the difficulty in these models comes from the coupling terms involving some derivatives of the unknown physical variables that make the system non-conservative and possibly non-hyperbolic. Due to these terms, a numerical scheme originally designed for single-layer shallow water equations will lead to instabilities when it is applied to each layer separately. In the present work we extend the finite volume modified method of characteristics developed by the authors in [3] to solve the density-driven multi-layer shallow water flows. The method avoids the solution of Riemann problems and belongs to the predictor-corrector type methods. The predictor stage uses the method of characteristics to reconstruct the numerical fluxes whereas, the corrector stage recovers the conservation equations. The proposed method is simple, conservative, non-oscillatory and suitable for multi-layer shallow water equations for which Riemann problems are difficult to solve. Numerical examples are presented to verify the considered multi-layer shallow water model. We demonstrate the model capability of calculating lateral and vertical distributions of velocities for density-driven multi-layer shallow water flow on flat bottom and over a hump.

The organization of the present paper is as follows. In section 2 we first give a brief description of the model employed for the multi-layer shallow water equations in density-driven flows. We then formulate the finite volume modified method of characteristics for the governing equations in section 3. This section includes the reconstruction of the numerical fluxes and the discretization of the source terms. Numerical results are presented in section 4 for several test examples in density-driven multi-layer shallow water flows. Section 5 contains concluding remarks and remarks about future work.

2 Equations for density-driven multi-layer shallow water flows

In the current study we are interested on density-driven flows occurring on the water free-surface where assumptions of shallow water flows applied. We consider the one-dimensional multi-layer shallow water equations written in a

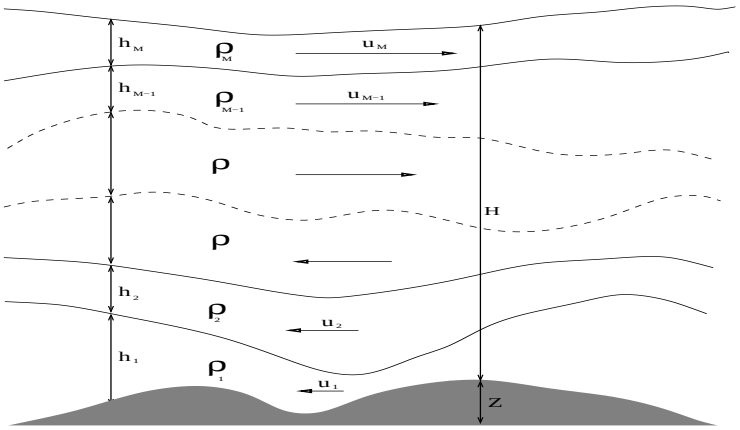

Fig. 1. Schematic of a multi-layer shallow water equations.

conservative form as

$$\begin{aligned} \partial_t \left(\rho_j h_j\right) + \partial_x \left(\rho_j h_j u_j\right) &= 0, \\ \partial_t \left(\rho_j h_j u_j\right) + \partial_x \left(\rho_j h_j u_j^2 + \frac{1}{2} g \rho_j h_j^2\right) &= -g\rho_j h_j \partial_x Z - \\ & g\rho_j h_j \sum_{k=1}^{j-1} \partial_x h_k - g h_j \sum_{k=j+1}^{M} \partial_x \left(\rho_k h_k\right), \end{aligned} \tag{1}$$

where $j = 1, \ldots, M$, with M is the total number of layers, ρ_j is the water density of the jth layer, $h_j(t,x)$ is the water height of the jth layer, $u_j(t,x)$ is the local water velocity for the jth layer, $Z(x)$ is the bottom topography and g the gravitational acceleration, see Figure 1 for a simplified representation. For two layers with constant density ρ_1 and ρ_2, the equations (1) reduce to the standard two-layer shallow water equations studied for example in [6]. In the current work, we assume that a sediment transport takes place such that the density depends on space and time variables, *i.e.*, $\rho_j = \rho_j(t,x)$. This requires additional equations for its evolution. Here, the equations used to close the system are given by

$$\rho_j = \rho_w + \left(\rho_{s_j} - \rho_w\right) c_j, \qquad j = 1, \ldots, M, \tag{2}$$

where ρ_{s_j} is the sediment density with $\rho_{s_j} > \rho_w$, and c_j is the depth-averaged concentration of the suspended sediment for the jth layer. The equation for mass conservation of species is modeled by

$$\partial_t \left(\rho_{s_j} h_j c_j\right) + \partial_x \left(\rho_{s_j} h_j u_j c_j\right) = 0, \qquad j = 1, \ldots, M. \tag{3}$$

For simplicity in presentation we rewrite the equations (1) and (3) in a compact conservative form as

$$\partial_t \mathbf{W} + \partial_x \mathbf{F}(\mathbf{W}) = \mathbf{Q}(\mathbf{W}), \tag{4}$$

where $\mathbf{W}$ is the vector of conserved variables, $\mathbf{F}$ the vector of flux functions and $\mathbf{Q}$ is the vector of source terms. For single-layer flows with variable density,

the equation (4) leads to the model for shallow water flows with variable horizontal density studied in [5]. Another multi-layer shallow water system with variable density has also been presented in [1]. This model does not account for conservation of species (3) and uses instead a Boussinesq approximation for dependence of the density on the temperature.

An equivalent system to the water flow equations (1) and the suspended sediment equations (3) can be obtained by using the physical variables as

$$\begin{aligned} D_t^{(j)}\left(\rho_j h_j\right) + \rho_j h_j \partial_x u_j &= 0, \\ D_t^{(j)} u_j + g\partial_x\left(Z + \frac{1}{2}h_j + \sum_{k=1}^{j-1} h_k\right) &= -\frac{g}{\rho_j}\partial_x\left(\frac{1}{2}\rho_j h_j + \sum_{k=j+1}^{M}\left(\rho_k h_k\right)\right), \\ D_t^{(j)}\rho_j &= 0, \qquad j = 1,\ldots,M, \end{aligned} \tag{5}$$

where $D_t^{(j)}$ denotes the total derivative defined as

$$D_t^{(j)}\omega = \partial_t\omega + u_j\partial_x\omega, \qquad j = 1,\ldots,M. \tag{6}$$

Note that $D_t^{(j)}\omega$ measures the rate of change of the function ω following the trajectories of the flow particles in the jth layer. We should also emphasize that it is not easy to confirm the hyperbolicity of the system (4). In the case of its single-layer counterpart, the authors in [5] have calculated the three eigenvalues of the system. The two-layer system with constant density is only conditionally hyperbolic, see for example [4,6] whereas, the multi-layer system with constant density in [1] is proven to be hyperbolic only for the two-layer case. It is worth remarking that the finite volume modified method of characteristics proposed in this paper does not require the explicit calculation of the eigenvalues of (4) and can be applied for arbitrary number M of the layers. In what follows we describe the different steps of the proposed finite volume modified method of characteristics.

3 Modified finite volume method of characteristics

Let us discretize the spatial domain into control volumes $[x_{i-1/2}, x_{i+1/2}]$ with uniform size $\Delta x = x_{i+1/2} - x_{i-1/2}$ and divide the temporal domain into subintervals $[t_n, t_{n+1}]$ with stepsize Δt. Here, $t_n = n\Delta t$, $x_{i-1/2} = i\Delta x$ and $x_i = (i+1/2)\Delta x$ is the center of the control volume. Integrating the system (4) with respect to space and time over the time-space control volume $[t_n, t_{n+1}] \times [x_{i-1/2}, x_{i+1/2}]$ we obtain the following semi-discrete equations

$$\mathbf{W}_i^{n+1} = \mathbf{W}_i^n - \Delta t\frac{\mathcal{F}_{i+1/2}^n - \mathcal{F}_{i-1/2}^n}{\Delta x} + \Delta t\mathcal{Q}_i^n, \tag{7}$$

where $\mathbf{W}_i^n$ is the space average of the solution $\mathbf{W}$ in the control volume $[x_{i-1/2}, x_{i+1/2}]$ and at time t_n, *i.e.*,

$$\mathbf{W}_i^n = \frac{1}{\Delta x} \int_{x_{i-1/2}}^{x_{i+1/2}} \mathbf{W}(t_n, x)\, dx,$$

and $\mathcal{F}_{i\pm1/2}^n = \mathbf{F}(\mathbf{W}_{i\pm1/2}^n)$ are the numerical fluxes at cell interfaces $x = x_{i\pm1/2}$ and time t_n. In (7), $\mathcal{Q}_i^n$ is the difference notation for the discretized source terms $\mathbf{Q}(\mathbf{W}_i)$ in (4). It should be pointed out that as with all explicit time stepping methods the theoretical maximum stable time step Δt is specified according to the Courant-Friedrichs-Lewy (CFL) condition

$$\Delta t = Cr \frac{\Delta x}{\max\limits_{j=1,\ldots,M} \left(\left|\lambda_j^n\right|, \left|\mu_j^n\right|, \left|\nu_j^n\right| \right)}, \tag{8}$$

where Cr is a constant to be chosen less than unity and λ_j, μ_j and ν_j are the eigenvalues associated with each layer separately defined as

$$\lambda_j = u_j - \sqrt{g h_j}, \qquad \mu_j = u_j, \qquad \nu_j = u_j + \sqrt{g h_j}, \qquad j = 1, 2, \ldots M.$$

The spatial discretization of the equation (7) is complete when a numerical construction of the numerical fluxes $\mathcal{F}_{i\pm1/2}^n$ and source terms $\mathcal{Q}_i^n$ is chosen. In general, the construction of the numerical fluxes requires a solution of Riemann problems at the interfaces $x_{i\pm1/2}$. From a computational viewpoint, this procedure is very demanding and may restrict the application of the method for which Riemann solutions are not available. Our objective in the present work is to extend a finite volume modified method of characteristics (FVC) proposed by the authors to solve canonical single-layer shallow water equations in [3] to the density-driven flow system (4). The FVC method is simple, easy to implement, and accurately solves the conservation equations without relying on Riemann problem solvers. The central idea of the FVC method consists of reconstructing the numerical fluxes $\mathcal{F}_{i\pm1/2}^n$ by integrating the advective system (5) along the characteristics defined by the water velocity at each layer. In this section we give a brief description of the FVC method for solving the system (4) and the reader is urged to see our previous work in [3] for detailed formulation and analysis of the FVC method.

3.1 Discretization of the flux gradients

To reconstruct the numerical fluxes $\mathcal{F}_{i\pm1/2}^n$ in (7), we consider the method of characteristics applied to the advective version of the system (5). The main idea behind the method of characteristics is to impose a regular grid at the new time level, and to backtrack the flow trajectories to the previous time level. At the old time level, the quantities that are needed are evaluated by

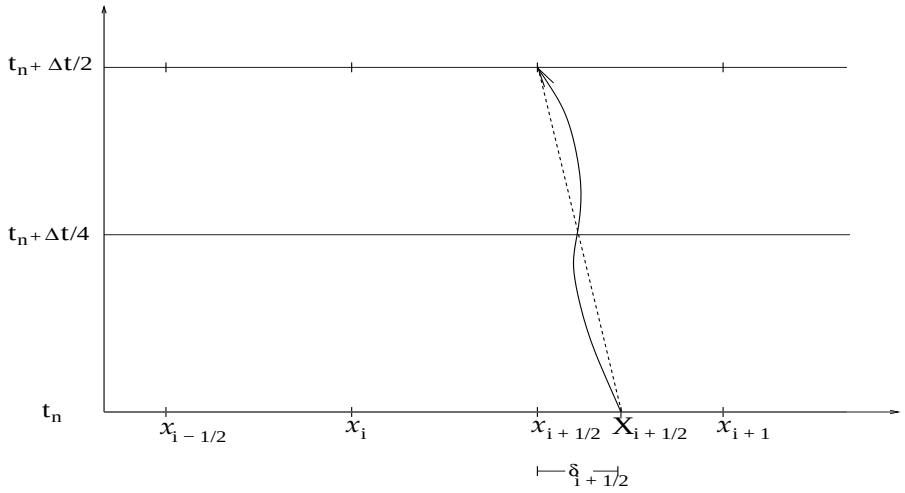

Fig. 2. A schematic diagram showing the control volumes and the main quantities used in the calculation of the departure points. The exact trajectory is represented by a solid line and the approximate trajectory with a dashed line.

interpolation from their known values on a regular grid, see for example [9,8]. Thus, the characteristic curves associated with the equation (5) are solutions of the initial-value problem

$$\begin{aligned} \frac{dX_{j,i+1/2}(\tau)}{d\tau} &= u_{j,i+1/2}\Big(\tau, X_{j,i+1/2}(\tau)\Big), \quad \tau \in [t_n, t_n + \Delta t/2]\,, \\ X_{j,i+1/2}(t_n + \Delta t/2) &= x_{i+1/2}, \qquad j = 1, 2, \ldots, M. \end{aligned} \tag{9}$$

Note that $X_{j,i+1/2}(\tau)$ is the departure point at time τ of a particle that will arrive at point $x_{i+1/2}$ in time $t_n + \Delta t/2$. The method of characteristics does not follow the flow particles forward in time, as the Lagrangian schemes do, instead it traces backward the position at time t_n of particles that will reach the points of a fixed mesh at time $t_n + \Delta t/2$. By doing so, the method avoids the grid distortion difficulties that the conventional Lagrangian schemes have, see for instance [9,8]. The solutions of (9) can be expressed as

$$\begin{aligned} X_{j,i+1/2}(t_n) &= x_{i+1/2} - \int_{t_n}^{t_n+\Delta t/2} u_{j,i+1/2}\left(X_{j,i+1/2}(\tau)\right) d\tau, \\ &= x_{i+1/2} - \delta_{j,i+1/2}, \qquad j = 1, 2, \ldots, M. \end{aligned} \tag{10}$$

It is worth remarking that the departure points in (10) are calculated in the interval $[t_n, t_n + \Delta t/2]$ instead of $[t_n, t_{n+1}]$. This is motivated by the idea of reconstructing a predictor-corrector scheme where the predictor stage is computed at the fractional time $t_n + \Delta t/2$ completed by a corrector stage computed at the end time t_{n+1}. This fractional time stepping is also supported by the analysis reported in [3].

To compute the displacement $\delta_{j,i+1/2}$ in (10) we consider the following iteration

$$\begin{aligned}
\delta^{(0)}_{j,i+1/2} &= \frac{\Delta t}{2} u_{j,i+1/2}\left(t_n, x_{i+1/2}\right), \\
\delta^{(m)}_{j,i+1/2} &= \frac{\Delta t}{2} u_{j,i+1/2}\left(t_n, x_{i+1/2} - \delta^{(m-1)}_{j,i+1/2}\right), \qquad m = 1, 2, \ldots.
\end{aligned} \tag{11}$$

The iterations (11) are terminated when the following criteria

$$\frac{\left\|\delta^{(m)}_j - \delta^{(m-1)}_j\right\|}{\left\|\delta^{(m-1)}_j\right\|} < \varepsilon, \tag{12}$$

is fulfilled for the L^∞-norm $\|\cdot\|$ and a given tolerance ε. It is also known [7] that

$$\left\|\delta_j - \delta^{(m)}_j\right\| \leq \frac{\Delta t}{8}\left\|\delta_j - \delta^{(m-1)}_j\right\| \max_{j=1,\ldots,M}\left(|\partial_x u_j|\right), \qquad m = 1, 2, \ldots. \tag{13}$$

Hence, a necessary condition for the convergence of iterations (11) is that the velocity gradient satisfies

$$\max_{j=1,\ldots,M}\left(|\partial_x u_j|\right)\Delta t \leq 8. \tag{14}$$

Note that the condition (14) is sufficient to guarantee that the characteristics curves do not intersect during a time step of size $\Delta t/2$. A schematic representation of the quantities involved in computing the departure points is shown in Figure 2.

Once the characteristics curves $X_{j,i+1/2}(t_n)$ are known, a solution at the cell interface $x_{i+1/2}$ is reconstructed as

$$\begin{aligned}
\omega^n_{j,i+1/2} &= \omega_j\left(t_n + \Delta t/2, x_{i+1/2}\right), \\
&= \omega_j\left(t_n, X_{j,i+1/2}(t_n)\right), \\
&:= \tilde{\omega}^n_{j,i+1/2},
\end{aligned} \tag{15}$$

where $\tilde{\omega}^n_{j,i+1/2}$ is the solution at the characteristic foot $X_{j,i+1/2}(t_n)$ computed by interpolation from the gridpoints of the control volume where the departure point resides *i.e.*

$$\tilde{\omega}^n_{j,i+1/2} = \mathcal{P}\Big(\omega_j\left(t_n, X_{j,i+1/2}(t_n)\right)\Big), \tag{16}$$

where $\mathcal{P}$ represents the interpolating polynomial. For instance, a Lagrange-based interpolation polynomials can be formulated as

$$\mathcal{P}\Big(\omega_j\left(t_n, X_{i+1/2}(t_n)\right)\Big) = \sum_k \mathcal{L}_k\left(X_{j,i+1/2}(t_n)\right)\omega^n_{j,k}, \tag{17}$$

with $\mathcal{L}_k$ are the Lagrange basis polynomials given by

$$\mathcal{L}_k(x) = \prod_{\substack{q=0 \\ q\neq k}} \frac{x - x_q}{x_k - x_q}.$$

Note that other interpolation procedures in (16) can also be applied. It should also be stressed that in general, the method of characteristics fails to conserve mass, compare [8] and further references are therein. However, in our FVC method the mass lost in the predictor step for calculating the intermediate stages $\mathbf{W}^n_{i\pm1/2}$ will be recovered in the corrector step (7). It is evident from the formulation (7) that the FVC method is mass conservative.

3.2 Discretization of the source terms

Applied to the equations (5), the characteristic solutions are given by

$$\begin{aligned}
r^n_{j,i+1/2} &= \tilde{r}^n_{j,i+1/2} - \frac{\nu}{2}\tilde{r}^n_{j,i+1/2}\left(u^n_{j,i+1} - u^n_{j,i}\right), \\
u^n_{j,i+1/2} &= \tilde{u}^n_{j,i+1/2} - \frac{\nu}{2} g \left(\left[Z + \frac{1}{2}h_j + \sum_{k=1}^{j-1} h_k \right]_{i+1} - \left[Z + \frac{1}{2}h_j + \sum_{k=1}^{j-1} h_k \right]_{i} \right) \\
&\quad - \frac{\nu}{2}\frac{g}{\tilde{\rho}^n_{j,i+1/2}} \left(\left[\frac{1}{2}\rho_j h_j + \sum_{k=j+1}^{M} (\rho_k h_k) \right]_{i+1} - \left[\frac{1}{2}\rho_j h_j + \sum_{k=j+1}^{M} (\rho_k h_k) \right]_{i} \right), \\
\rho^n_{j,i+1/2} &= \tilde{\rho}^n_{j,i+1/2}, \qquad\qquad j = 1, \ldots, M,
\end{aligned} \tag{18}$$

where $r_j = \rho_j h_j$, $\nu = \frac{\Delta t}{\Delta x}$, $\tilde{r}^n_{j,i+1/2}$, $\tilde{u}^n_{j,i+1/2}$ and $\tilde{\rho}^n_{j,i+1/2}$ are the solutions at the characteristic foot computed by interpolation from the gridpoints of the control volume where the departure points $X_{j,i+1/2}(t_n)$ are located. The numerical fluxes $\mathcal{F}_{i\pm1/2}$ in (7) are calculated using the intermediate states $\mathbf{W}^n_{i\pm1/2}$ recovered accordingly from the characteristic solutions in (18). Hence, the FVC method (7) reduces to

$$\begin{aligned}
r^{n+1}_{j,i} &= r^n_{j,i} - \nu\left((r_j u_j)^n_{i+1/2} - (r_j u_j)^n_{i-1/2} \right), \\
q^{n+1}_{j,i} &= q^n_{j,i} - \nu \left(\left[\rho_j h_j u_j^2 + \frac{1}{2} g \rho_j h_j^2 \right]^n_{i+1/2} - \left[\rho_j h_j u_j^2 + \frac{1}{2} g \rho_j h_j^2 \right]^n_{i-1/2} \right) \\
&\quad - \frac{1}{2}\nu g \hat{r}^n_{j,i} \left(\left[Z + \sum_{k=1}^{j-1} h_k \right]_{i+1} - \left[Z + \sum_{k=1}^{j-1} h_k \right]_{i-1} \right), \\
&\quad - \frac{1}{2}\nu g \hat{h}^n_{j,i} \left(\left[\sum_{k=j+1}^{M} (\rho_k h_k) \right]_{i+1} - \left[\sum_{k=j+1}^{M} (\rho_k h_k) \right]_{i-1} \right), \\
\sigma^{n+1}_{j,i} &= \sigma^n_{j,i} - \nu\left((\sigma_j u_j)^n_{i+1/2} - (\sigma_j u_j)^n_{i-1/2} \right),
\end{aligned} \tag{19}$$

where $r_j = \rho_j h_j$, $q_j = r_j u_j$ and $\sigma_j = \rho_{s_j} h_j c_j$, with $j = 1, \ldots, M$. In our FVC method, the reconstruction of the terms $\hat{h}^n_{j,i}$ and $\hat{r}^n_{j,i}$ in (19) are carried out such that the discretization of the source terms is well balanced with the discretization of flux gradients using the same concept as in [3] by

$$\hat{h}^n_{j,i} = \frac{1}{4}\left(h^n_{j,i+1} + 2h^n_{j,i} + h^n_{j,i-1}\right), \qquad \hat{r}^n_{j,i} = \frac{1}{4}\left(r^n_{j,i+1} + 2r^n_{j,i} + r^n_{j,i-1}\right).$$

In summary, the implementation of FVC algorithm to solve the density-driven multi-layer shallow water equations (4) is carried out in the following steps. Given $\left(h^n_{j,i}, q^n_{j,i}, \sigma^n_{j,i}\right)$, we compute $\left(h^{n+1}_{j,i}, q^{n+1}_{j,i}, \sigma^{n+1}_{j,i}\right)$ via:

Step 1. *Calculate the departure points $X_{j,i+1/2}(t_n)$, with $j = 1, \ldots, M$ using the iterative procedure* (10)-(11).

Step 2. *Compute the approximations*

$$\tilde{h}^n_{j,i+1/2} = h_j\left(t_n, X_{j,i+1/2}(t_n)\right), \qquad \tilde{u}^n_{j,i+1/2} = u_j\left(t_n, X_{j,i+1/2}(t_n)\right),$$

$$\tilde{\rho}^n_{j,i+1/2} = \rho_j\left(t_n, X_{j,i+1/2}(t_n)\right),$$

employing an interpolation procedure.

Step 3. *Evaluate the intermediate states $r^n_{j,i+1/2}$, $u^n_{j,i+1/2}$ and $\rho^n_{j,i+1/2}$ from the predictor stage* (18).

Step 4. *Update the species concentration $c^n_{j,i+1/2}$ using the equation* (2) *as*

$$c^n_{j,i+1/2} = \frac{\rho^n_{j,i+1/2} - \rho_w}{\rho_{s_j} - \rho_w}.$$

Step 5. *Compute the conservation solutions $r^{n+1}_{j,i}$, $q^{n+1}_{j,i}$ and $\sigma^{n+1}_{j,i}$ using the corrector stage* (19).

Note that other interpolation procedures in Step 2 can also be applied. In our simulations we have used a linear interpolation since for this type of interpolations the obtained solution remains monotone and the FVC method preserves the exact water equilibrium at the machine precision, compare [3].

4 Numerical results and applications

In this section we present numerical results obtained for two test examples for density-driven shallow water flows over both a flat and a non-flat bottom. The main goals of this section are to illustrate the numerical performance of the FVC method described above and to verify numerically its capabilities to solve shallow water flows with variable density on a non-flat bottom. In all the computations reported herein, the gravity acceleration $g = 9.81\ m/s^2$, the

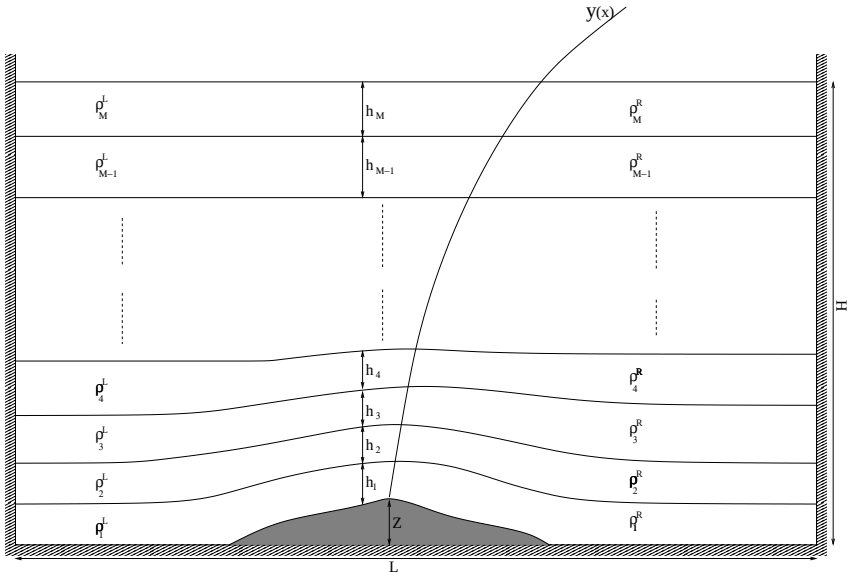

Fig. 3. Configuration for the flow system used in the simulations.

Courant number Cr is set to 0.5 and the time stepsize Δt is adjusted at each step according to the CFL condition (8).

We consider a test example of multi-layer density-driven flow problem in a rectangular channel of length 100 m, see Figure 3 for a sketch. The total water height in the channel is set to $H = 10\ m$ and discretized into M superposed layers such that the first 4 layers are selected to be within a height $b = 3\ m$ close to the bottom *i.e.*

$$h_j(t,x) = \begin{cases} \dfrac{b - Z(x)}{4}, & \text{if} \quad j \leq 4, \\ \dfrac{H-b}{M-4}, & \text{otherwise.} \end{cases} \tag{20}$$

For the water density distribution we assume horizontal and vertical variations are taken place in the channel. As shown in Figure 3, the discontinuity in the water densities is located at a parabolic interface $y(x)$ defined by

$$y(x) = 0.03x^2 + 0.01x - 8.$$

Thus, given the left upper density $\rho_L^U = 900\ kg/m^3$, the right upper $\rho_R^U = 1010\ kg/m^3$, the left lower density $\rho_L^L = 990\ kg/m^3$ and the right lower density $\rho_R^L = 1100\ kg/m^3$, the initial water density $\rho_j(t,x)$ at each layer j is given by

$$\rho_j(t,x) = \begin{cases} \rho_L^L - (j-1)\Delta\rho^L, & \text{if} \quad x < y(x), \\ \rho_R^L - (j-1)\Delta\rho^R, & \text{if} \quad x > y(x), \end{cases} \tag{21}$$

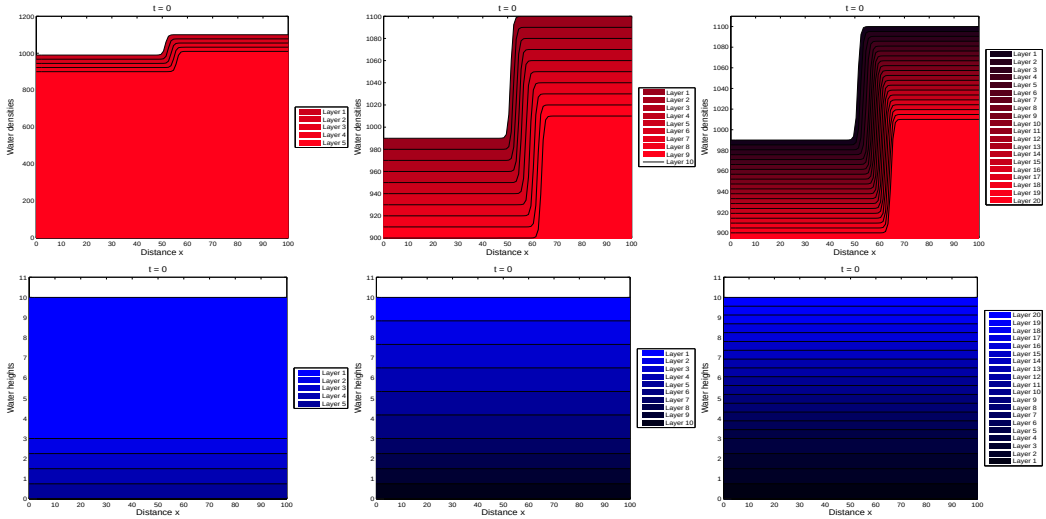

Fig. 4. Initial water densities (top) and water heights (bottom) for the 5-layer model (left) 10-layer model (middle) and 20-layer model (right) on a flat bottom.

where the density increments $\Delta\rho^L$ and $\Delta\rho^R$ are defined as

$$\Delta\rho^L = \frac{\rho_L^L - \rho_L^U}{M-1}, \qquad \Delta\rho^R = \frac{\rho_R^L - \rho_R^U}{M-1}.$$

This variation in the water density can be interpreted by the variation of water temperature or water salinity with the water depth in the channel and as a consequence the main flow is governed by the density variation. In our simulations, the computational domain is discretized into 100 control volumes and wall boundary conditions are implemented. The system is assumed to be at rest and at $t = 0$ the interface collapses and the flow problem consists of a shock wave traveling downstream and a rarefaction wave traveling upstream. These flow features are well-established for the canonical dam-break flow problems.

4.1 Density-driven flow on a flat bottom

First we present numerical results obtained on flat bottom *i.e.* $Z(x) = 0$. In Figure 4 we display the initial conditions for water densities and water heights associated with 5-layer, 10-layer and 20-layer shallow water models. We have used different color scales to differentiate between the layers with a darker color refers to the layers close to the channel bed. We apply the multilayer shallow equations (4) to these initial conditions and numerical results are displayed at three different instants namely, $t = 30\ s$, $120\ s$, and $240\ s$. Figure 5 presents the results obtained for the 5-layer model. Those results obtained for the 10-layer and 20-layer models are illustrated in Figure 6 and Figure 7, respectively. In these figures we show the snapshots of the water

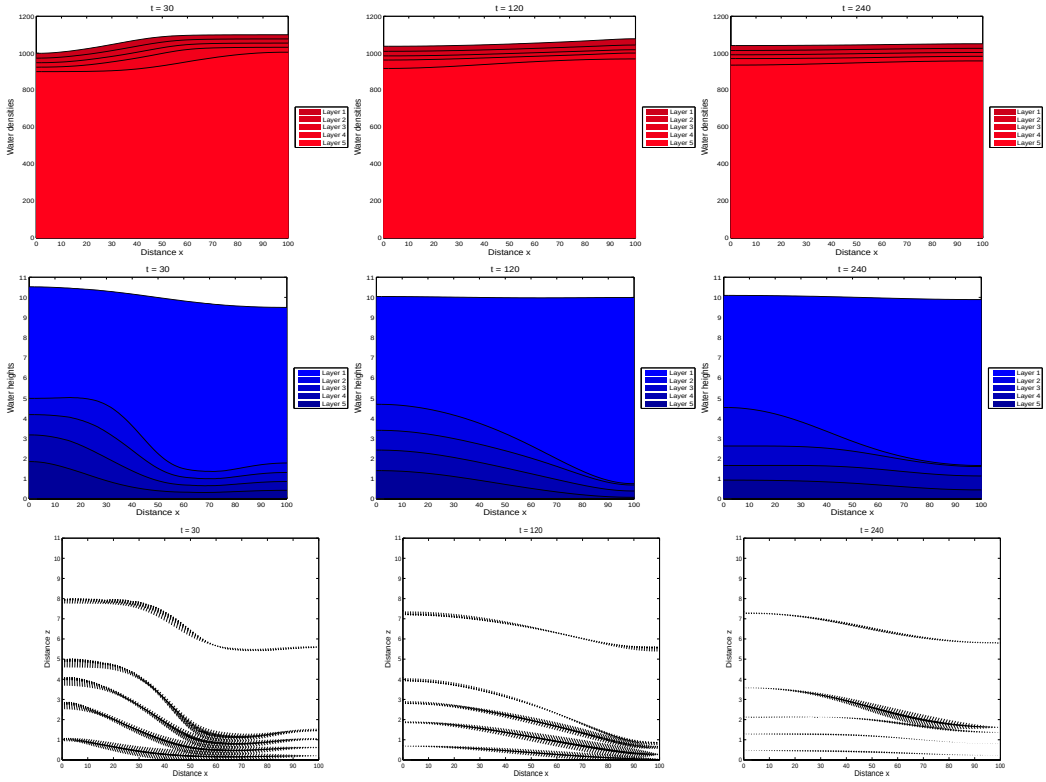

Fig. 5. Water densities (top), water heights (middle) and velocity fields (bottom) for the 5-layer model on a flat bottom. From left to right $t = 30$ s, 120 s, and 240 s.

densities, water heights and water velocity fields. It should be stressed that for the presented velocity fields, the vertical velocity is calculated using the divergence-free condition in the flow system along with the method described in [2].

For all considered layers, we observe that the variation in the water density results in moving fronts with different speeds and different amplitudes traveling in the channel. Obviously, the free-surface trends in the considered multi-layer models look similar however, the velocity fields exhibit different flow features. Observe the recirculation zones appeared in the velocity fields obtained using the 10-layer and the 20-layer models. The 5-layer model fails to capture the vertical effects for the water dynamics in the considered flow system. We have also noted that the 5-layer model produces diffusive water density and free-surface profiles. This diffusion has been reduced in the water density and free-surface results obtained using the 10-layer and 20-layer models. It is evident that the more layers used in the simulation the more accurate description of the vertical flow effects become. For example, using the 20-layer model the response of the upper free-surface layer to the vertical dynamics is more pronounced than using the 10-layer model, compare the velocity fields in Figure 7. The FVC method performs well for this unsteady multi-layer shallow water problem and produces accurate solutions without requiring special treatment

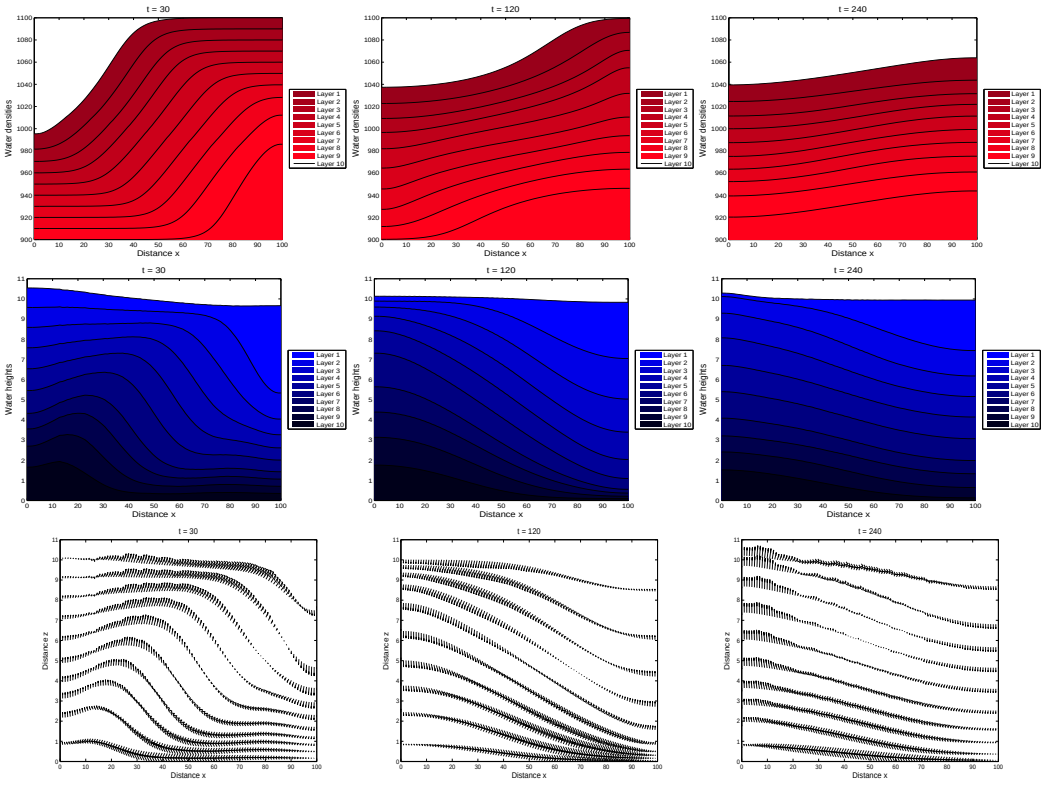

Fig. 6. The same as Figure 5 but for the 10-layer model on a flat bottom.

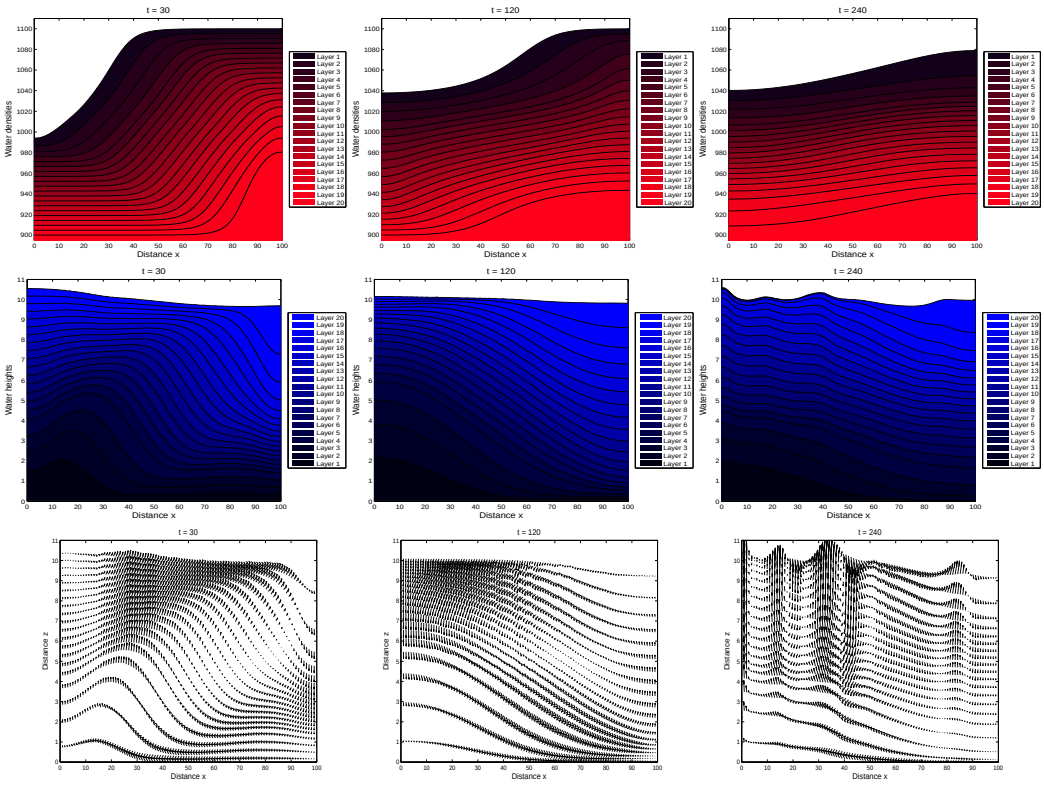

Fig. 7. The same as Figure 5 but for the 20-layer model on a flat bottom.

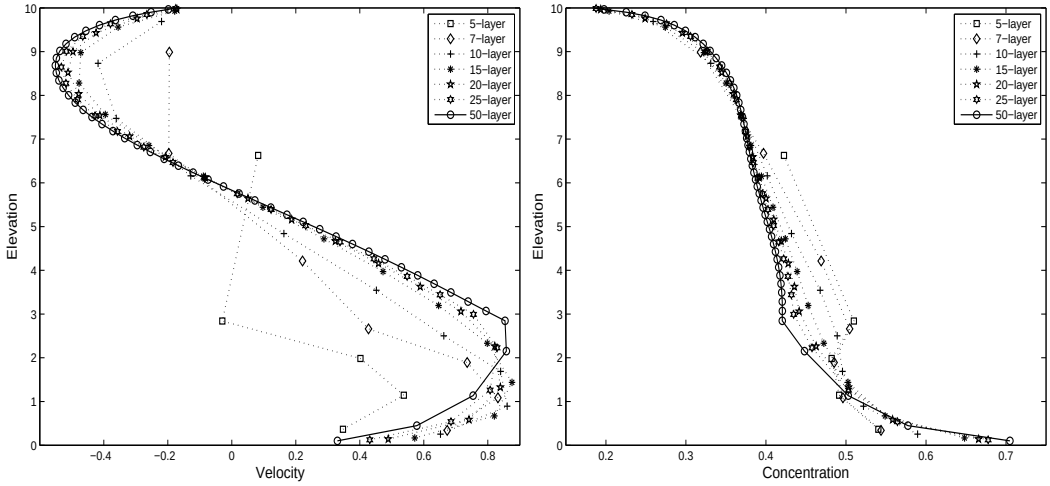

Fig. 8. Water velocity (left) and species concentration (right) at the mid channel $x = 50\ m$ for the multi-layer model on a flat bottom.

of the source terms or complicated upwind discretization of the gradient fluxes.

For visualizing the comparisons, we display in Figure 8 the water velocity and the species concentration associated with each layer at the mid of the channel ($x = 50\ m$) for different multi-layer models at time $t = 120\ s$. Under the actual flow conditions, it is clear that the cross section plots exhibited different behaviors in the channel center and the results obtained for the 50-layer model are the most accurate. Similar features have been observed for a comparison, not reported here, of cross sections for water heights and water densities. As expected for low number of layers in the flow system, the vertical effects may not be clearly captured. Note that these flow features are impossible to recover using the single-layer model studied in [5]. The computed results also verify the stability and the well-balanced properties of the considered finite volume modified method of characteristics. The proposed FVC method performs very satisfactorily for this multi-layer flow problem since it does not diffuse the moving fronts and no spurious oscillations have been detected near steep gradients of the flow field and water density in the computational domain.

4.2 Density-driven flow over a hump

Now we turn our attention to the test example of density-driven flow over a hump defined by

$$Z(x) = e^{-\frac{(x-50)^2}{200}}.$$

The initial conditions for water densities and water heights are depicted in Figure 9 for the considered 5-layer, 10-layer and 20-layer shallow water models.

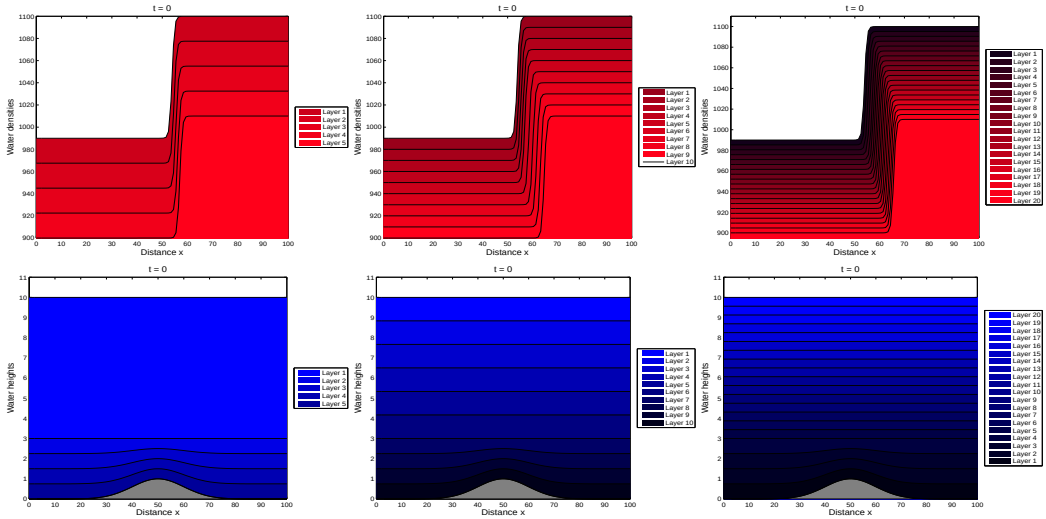

Fig. 9. Initial water densities (top) and water heights (bottom) for the 5-layer model (left) 10-layer model (middle) and 20-layer model (right) over a hump.

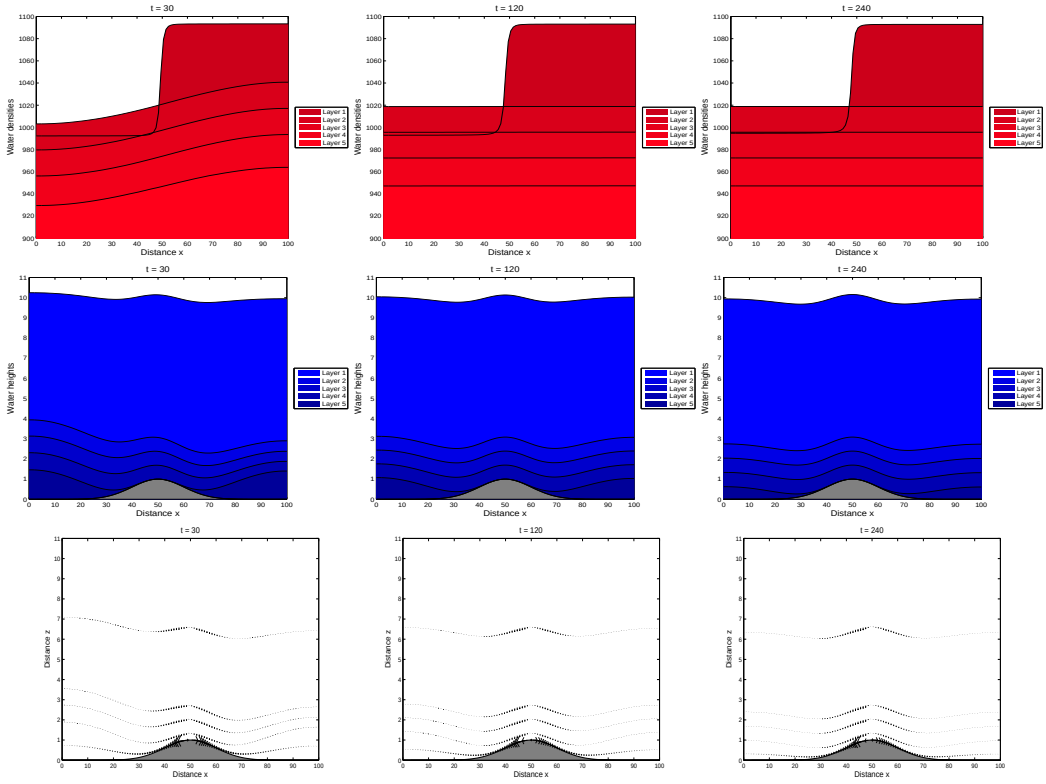

Fig. 10. Water densities (top), water heights (midlle) and velocity fields (bottom) for the 5-layer model over a hump. From left to right $t = 30\ s$, $120\ s$, and $240\ s$.

In Figure 10 we present the time evolution of the water densities, water heights and water velocity fields at $t = 30\ s$, $120\ s$, and $240\ s$ for the 5-layer model. Those results obtained for the 10-layer and 20-layer models are illustrated in Figure 11 and Figure 12, respectively. It is clear that using the conditions for

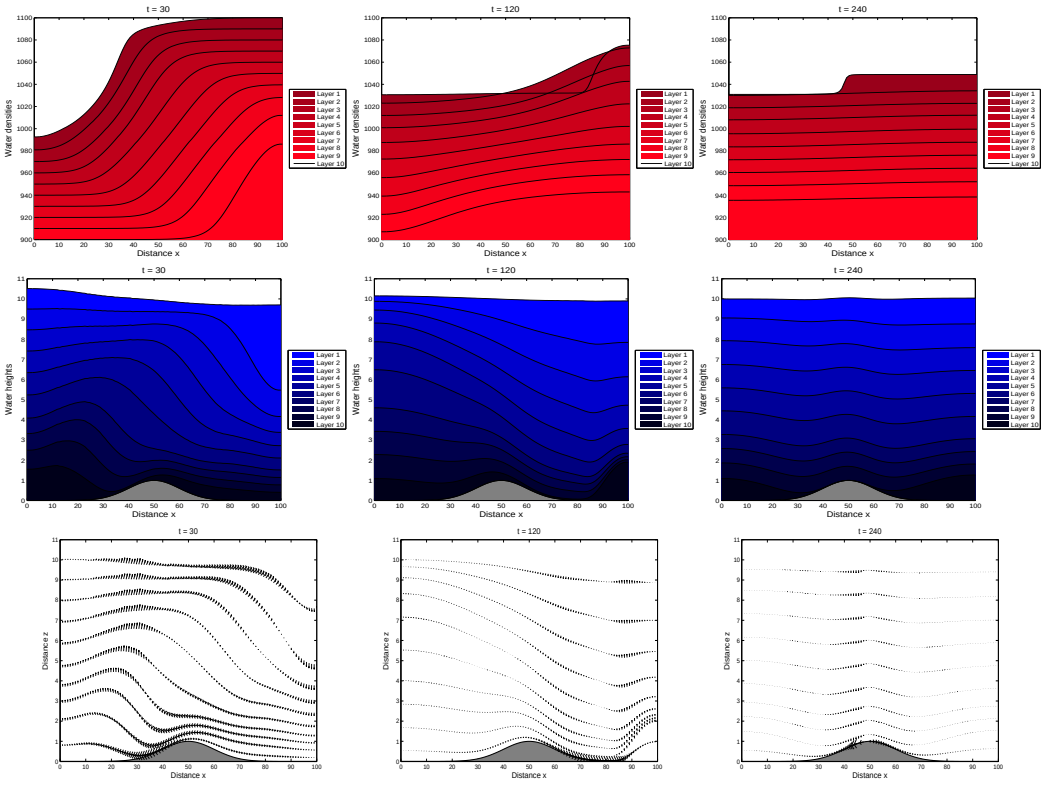

Fig. 11. The same as Figure 10 but for the 10-layer model over a hump.

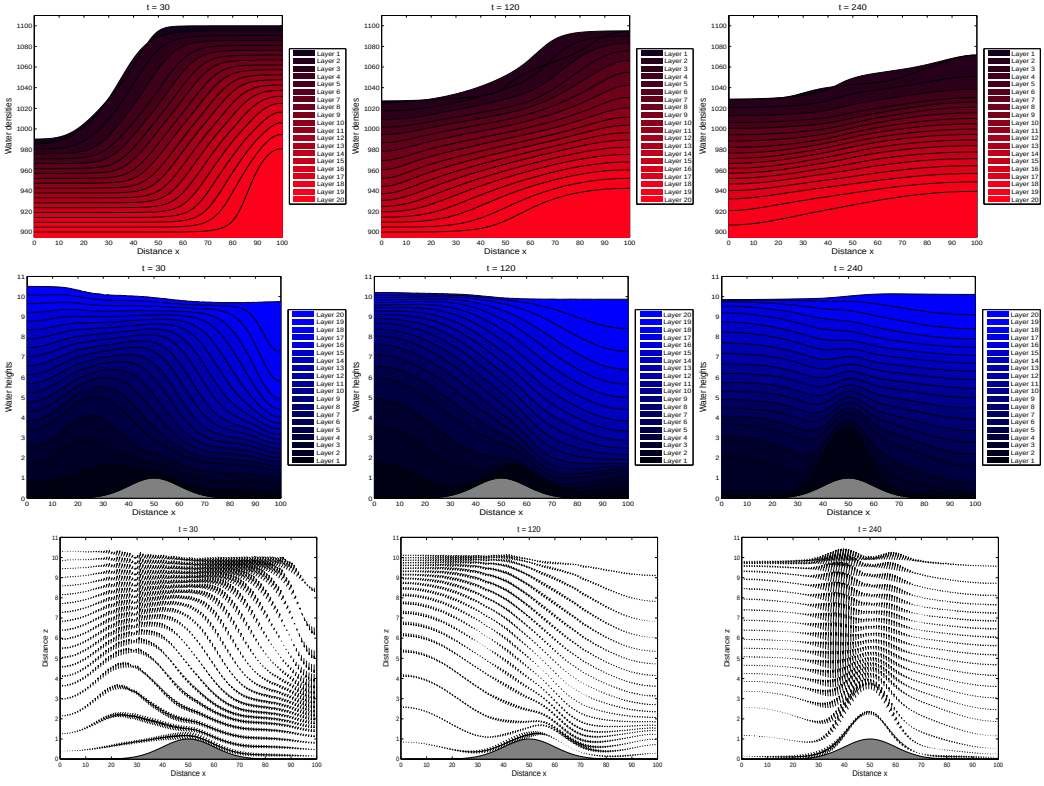

Fig. 12. The same as Figure 10 but for the 20-layer model over a hump.

the density-driven flow problem and the considered bottom topography, the flow exhibits a recirculation zone with different order of magnitudes over the hump. At the beginning of simulation time, the water flows over the hump and moves towards the channel walls. At later time, due to the boundary conditions imposed on the walls, the water flow changes the direction and a water soliton is formed and it propagates over the hump. As can be seen, the response of the water free-surface to the bottom bed is more pronounced for the 5-layer model that the other 10-layer and 20-layer models.

Again, the proposed FVC scheme performs well for this density-driven flow problem since it does not diffuse the moving fronts and no spurious oscillations have been observed when the water flows over the hump. Note that the performance of the proposed FVC method is very attractive since the computed solutions remain stable and oscillation-free even for coarse grids without solving nonlinear systems or Riemann problems.

5 Conclusions

we have proposed a simple and accurate finite volume modified method of characteristics to solve multi-layer shallow water equations for density-driven flows. The proposed finite volume method consists of two stages which can be viewed as a predictor-corrector procedure. In the first stage, the scheme reconstructs the numerical fluxes using the method of characteristics. This stage results in an upwind discretization of the characteristic variables and avoids the Riemann problem solvers. In the second stage, the solution is updated using the conservation system. The method combines the attractive attributes of the finite volume discretization and the method of characteristics to yield a robust algorithm for multi-layer density-driven shallow water flows. The method does not require either nonlinear solution or special treatment of the bed bottom. The proposed method has been numerically examined for the test example of density-driven flow problem on a both flat and a non-flat topography. The obtained results have exhibited accurate prediction of both, the water free-surface and the water velocity field with correct dynamics, and stable representation of free-surface response to the variation in the water density. The results make it promising to be applicable also to real situations where, beyond the many sources of complexity, there is a more severe demand for accuracy in predicting density-driven shallow water flows, which must be performed for long time.

We conclude with some comments on the current development of this finite volume method, in terms of both physical and numerical features that will be implemented. In this paper, we have only considered source terms due to the bottom topography. However, in many hydraulic scenarios, mass ex-

changes, friction losses and viscous terms, which interact with the hydraulics through the introduction of stress terms in the momentum equations, can be the dominant force in the multi-layer shallow water equations for density-driven flows. Therefore, future work will involve inclusion of viscous coupling a wave model component into the modelling system to include the effects of bottom friction, wind stresses, eddy viscosity, and mass exchange in the multi-layer density-driven flows. Numerically, the present scheme is a suite of finite volume modified method of characteristics that are currently being developed. Other method components will include application to tidal flows and lock exchange flows. In many situations, these models will be solved on large domains and over irregular bathymetries such as coastal scenarios. The proposed finite volume modified method of characteristics is particularly advantageous for this class of applications.

Acknowledgment. The authors would like to thank Prof. E. Audusse for valuable discussions about the modelling aspect of the multi-layer shallow water flows.

References

[1] E. Audusse, M.-O. Bristeau, M. Pelanti, J. Sainte-Marie, Approximation of the hydrostatic Navier-Stokes system for density stratified flows by a multilayer model: Kinetic interpretation and numerical solution, *J. Comput. Physics.*, **230**, 3453–3478 (2011).

[2] E. Audusse, M.-O. Bristeau, M. Pelanti, J. Sainte-Marie, A multilayer Saint-Venant system with mass exchanges for Shallow Water flows. Derivation and Numerical Validation, *M2AN Math. Model. Numer. Anal.*, **45**, 169–200 (2011).

[3] F. Benkhaldoun and M. Seaïd, A simple finite volume method for the shallow water equations, *J. Comp. Applied Math.*, **234**, 58–72 (2010).

[4] D. Farmer and L. Armi, Maximal two-layer exchange over a sill and through a combination of a sill and contraction with barotropic flow, *J. Fluid Mech.*, **164**, 53–76 (1986).

[5] Leighton F.Z, Borthwick A.G.L, Taylor P.H, 1-D numerical modelling of shallow flows with variable horizontal density. *International Journal for Numerical Methods in Fluids* 2010; **62**:1209–1231

[6] M.J. Castro, J.A. García-Rodrguez, J.M. González-Vida, J. Macías, C. Parés and M.E. Vázquez-Cendón, Numerical simulation of two-layer shallow water flows through channels with irregular geometry, *J. Comp. Physics.*, **195**, 202–235 (2004).

[7] J. Pudykiewicz and A. Staniforth, Some properties and comparative performance of the semi-Lagrangian method of Robert in the solution of advection-diffusion equation, *Atmos. Ocean.*, **22**, 283–308 (1984).

[8] M. Seaïd, On the quasi-monotone modified method of characteristics for transport-diffusion problems with reactive sources. Comp. Methods in App. Math. 2 (2002) 186–210.

[9] C. Temperton, A. Staniforth, An efficient two-time-level semi-Lagrangian semi-implicit integration scheme. Quart. J. Roy. Meteor. Soc. 113 (1987) 1025–1039.